The α↔ω phase transformations and thermal stability of Ti—Co alloy treated by high pressure torsion

A. Korneva [a,*], B.B. Straumal [b,c], A.R. Kilmametov [f], Ł. Gondek [d], A. Wierzbicka-Miernik [a], L. Lityńska-Dobrzyńska [a], R. Chulist [a], G. Cios [e], P. Zięba [a]

[a] Institute of Metallurgy and Materials Science, Polish Academy of Sciences, 30-059 Krakow, Poland
[b] Karlsruhe Institute of Technology (KIT), Institute of Nanotechnology, 76344 Eggenstein-Leopoldshafen, Germany
[c] Institute of Solid State Physics, Russian Academy of Sciences, 142432 Chernogolovka, Russia
[d] GH University of Science and Technology, Faculty of Physics and Applied Computer Science, Mickiewicza 30, 30-059 Kraków, Poland
[e] AGH University of Science and Technology, Academic Centre of Materials and Nanotechnology, Mickiewicza 30, 30-059 Kraków, Poland
[f] Scientific Center in Chernogolovka, Russian Academy of Sciences, 142432 Chernogolovka, Russia

ARTICLE INFO

Keywords:
Ti-based alloy
High pressure torsion
Phase transformations
High temperature X-ray diffraction
Transmission electron microscopy
Differential scanning calorimeter

ABSTRACT

The Ti–3.3 at.% Co was annealed at three different temperatures (400, 500 and 600 °C) in order to obtain (α + Ti_2Co) state with different concentrations of cobalt in the α-phase and the different volume fractions of Ti_2Co intermetallic particles. Next, the alloy was subjected to high pressure torsion (HPT) at room temperature. The deformed alloy was studied using X-ray diffraction, scanning and transmission electron microscopy. This showed strong microstructure grain refinement, fragmentation and partial Ti_2Co intermetallic phase dissolution, along with α → ω phase transformation. The volume fraction of the ω-phase depends strongly on the cobalt content in the initial α-matrix and the morphology of the α- and Ti_2Co phases. The thermal stability of the ω-phase was studied using calorimetric and *in situ* XRD measurements. It was found that the alloying of titanium with 3.3 at.% of cobalt results in a significant increase of the volume fraction of the ω-phase and its thermal stability from 180°C to 415°C in comparison to pure titanium.

1. Introduction

Ti–Co-based alloys are applied for many purposes, especially in dentistry and medicine [1], because alloying with Co improves corrosion resistance [2] and some mechanical properties [3]. It also reduces the melting temperature of titanium, which can resolve many casting problems. Nevertheless, new approaches are still required for further improvement of properties, especially mechanical ones. It is well known that the methods of severe plastic deformation (SPD) allow the production of bulk nanomaterials with unique mechanical properties due to the strong grain refinement of their microstructure. On the other hand, SPD can, under certain conditions, cause some phase transformation such as the formation or decomposition of a supersaturated solid solution [4,5], dissolution of phases [6], amorphisation of crystalline phases [7], decomposition of the amorphous phase with the formation of nanocrystals [8], or allotropic phase transformations [9]. SPD-driven phase transformations are especially effective for titanium since it possesses three allotropic variations: low-temperature α-Ti with a hexagonal close-packed crystal structure (space group P63/mmc), high-temperature β-Ti with a body-centred cubic structure (space group Im3m), and high-pressure ω-Ti with a hexagonal structure (space group P6/mmm). It was found that, in the Ti-based alloys, the ω-Ti phase forms more easily from the β-Ti phase during SPD [10], and also from the α-Ti phase under pressure between 2 and 8 GPa, depending on the experimental technique, pressure and alloying additions [11]. The formation of the ω-phase in Ti is related to the specific electronic structure, which is characterized by the relationship between the occupied narrow *d* bands and the broad *sp* bands. Under pressure, the *sp* bands rise faster in energy, causing electrons to be transferred to the *d* bands [12]. This process is known as the *s-d* transition, and it governs the structural properties of the transition metals. It was found that external shear stress and the alloying of pure Ti with β-stabilising elements such as the *d*-electron-rich transition elements (for example, Co, V, Mo, Fe, Ni or Nb), provide an additional driving force for α → ω or β → ω transformations [13]. After HPT, the ω-to-α reverse phase transformation kinetics in pure Ti [14] and the thermal stability of the ω-phase in Ti—Fe alloys [15]

* Corresponding author at: Institute of Metallurgy and Materials Science, Polish Academy of Sciences, 25 Reymonta Street, 30-059 Krakow, Poland.
E-mail address: a.korniewa@imim.pl (A. Korneva).

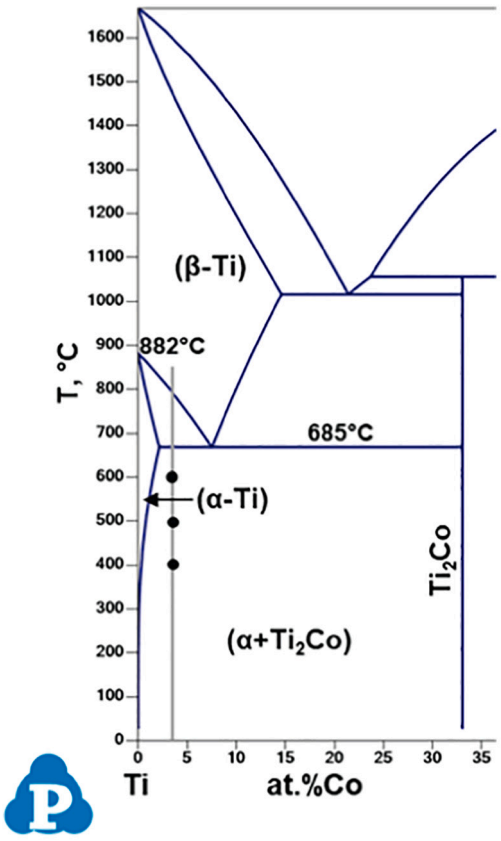

Fig. 1. The Ti-rich part of the Ti—Co phase diagram. The gray vertical line shows the composition of the Ti–3.3 at.% Co alloy; the black rounds show the temperatures of annealing. The phase diagram was calculated based on the database from Ref. [18].

were studied. However, there is still a lack of detailed knowledge about the fundamentals of ω-phase formation under the influence of HPT and about the thermal stability of the ω-phase in Ti-Co-based alloys. The initial state containing the mixture of α-phase and intermetallic compound instead of (α + β)-phase composition [17] is of special interest. Therefore, the main ongoing aims of this work were the study of fundamentals of the α → ω phase transformation caused by the HPT in Ti–3.3 at.% Co alloy, as well as the study of the ω-phase thermal stability and the influence of ω-phase formation on the microhardness of the alloy.

2. Material and methods

Pure titanium (99.98%) and cobalt (99.99%) were used for preparation of the Ti–3.3 at.% Co alloy. The concentration of 3.3 at.% Co is shown on the left side of the point of eutectoid β → α + Ti_2Co transformation (see Fig. 1). The alloy was melted in an induction furnace in a pure argon atmosphere. The obtained cylindrical ingots of the alloy with a diameter of 10 mm were cut by spark erosion into discs with a thickness of 0.7 mm. The samples were then sealed in quartz ampoules and annealed at temperatures of 400, 500 and 600 °C (for 5685, 5685, and 2774 h, respectively) in a vacuum at a residual pressure of 4×10^{-4} Pa. The samples were annealed for such a very long time in order to reach the equilibrium cobalt content in the α-solid solution. After annealing, the samples, together with their ampoules, were quenched in water. The annealed samples were subjected to HPT at room temperature under pressure of 7 GPa for five full rotations with a deformation rate of 1 rpm, in a Bridgman anvil type unit using a custom computer-controlled device manufactured by W. Klement GmbH, Lang, Austria. After HPT, the thickness of the samples was 0.35 mm. X-ray diffraction (XRD) studies were carried out using a Siemens D-500 X-ray diffractometer with Cu-Kα radiation. Lattice parameter evaluation was performed using Fityk software [28] with Rietveld-like whole profile refinement. Transmission electron microscopy (TEM) investigations were carried out using a TECNAI G2 FEG super TWIN (200 kV) with an energy dispersive X-ray (EDS) spectrometer manufactured by EDAX. The thin foils for TEM observation were prepared using a twin-jet polishing technique with a D2 electrolyte manufactured by Struers. Prior inspection of the obtained material was also carried out using an FEI *E*-SEM XL30 scanning electron microscope equipped with EDAX Genesis EDS spectrometer. The SEM images were taken using backscattered electron signal (BSE mode) in order to obtain the composition contrast between different phases. All the microstructural studies were cut out at a distance of half the radius of the deformed samples due to the heterogeneity of the microstructure along the diameter of the deformed samples. *In situ* XRD studies were carried out using a Panalytical Empyrean diffractometer (Cu-*Kα* radiation) equipped with an Anton Paar HTK 1200 high-temperature chamber. The bulk samples were placed on an Al_2O_3 sample holder and introduced into the chamber, which was

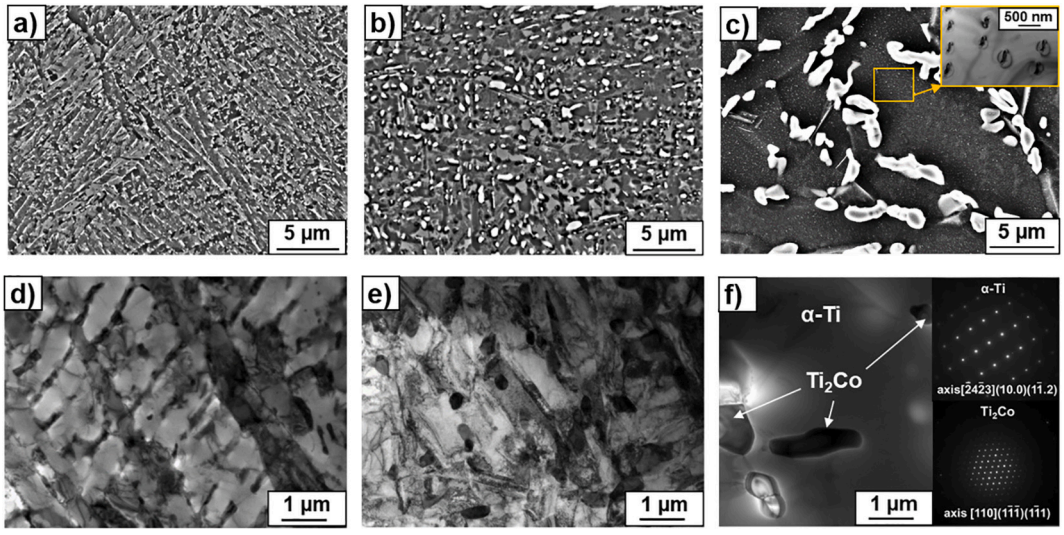

Fig. 2. SEM (a, b, c) and TEM (d, e, f) images of microstructure of the Ti–3.3 at.% Co alloy after annealing at 400 (a, d), 500 (b, e) and 600 °C (c, f). TEM image of the matrix at 600 °C is presented in the rectangle placed in the upper right corner of the Fig. 2c.

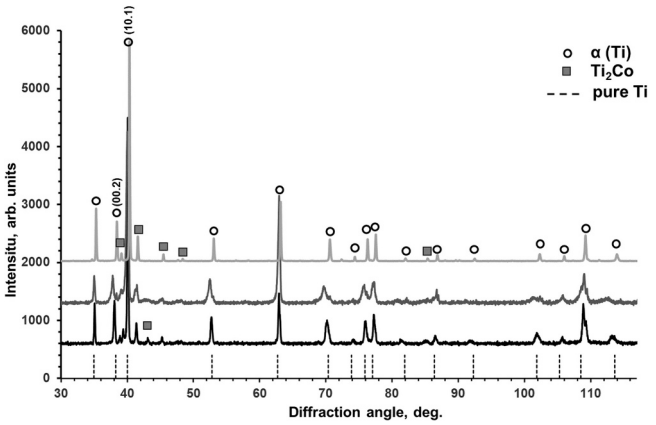

Fig. 3. X-ray diffraction patterns of the Ti–3.3 at.% Co alloy after annealing at 400, 500 and 600 °C. Vertical dotted lines show the positions of the reflections for pure titanium.

consequently evacuated, then flushed and filled with high purity (6 N) Ar gas. During measurements, the thermal displacement of the samples was cancelled by the appropriate movement of the chamber. Samples were heated at a rate of 5 °C/min, and diffraction patterns were collected at steps of 20 °C up to 800 °C. The 2θ range was chosen between 30 °C and 80 °C with step size of 0.01667°. The acquisition time per single pattern was 80 min. The collected data were refined using Rietveld-type FullProf software [18]. Differential scanning calorimetry (DSC) was carried out using a 404 F1 Pegasus, Netzsch equipment. The samples were heated to 800 °C in an argon atmosphere, in Al_2O_3 crucibles, at a rate of 20 °C/min. The hardness was measured using an AGILENT G200 nanoindenter with XP head at a load of 96 mN. The hardness was measured along the radius (from the centre to the edge) of the deformed discs with a step of 250 μm. Each hardness value was an average of 10 measurements.

3. Results and discussion

The SEM and TEM images of microstructure of the Ti–3.3 at.% Co alloy after annealing at 400, 500 and 600 °C are presented in Fig. 2. The microstructure contains large precipitates of the secondary phase, which are uniformly distributed in the α (Ti)-matrix. They were identified as the intermetallic Ti_2Co phase by selected area electron diffractions patterns (SAED). An example of solved SAED patterns is presented in Fig. 2f. The presence of the Ti_2Co phase was also confirmed by XRD analysis (Fig. 3). The morphology of observed microstructures is different: the lower the annealing temperature, the smaller the grain size of the α-phase and Ti_2Co particles (Fig. 2a-c). Moreover, at a temperature of 400°C, the particles were elongated and formed a network similar to cellular structure (Fig. 2d), while at higher temperatures they have a more circular shape and were not connected to each other. Small precipitates dispersed in the matrix were additionally observed in the sample annealed at 600 °C (Fig. 2c). As the SEM images were taken in the backscattered electron mode, where the atoms with high atomic number have a bright contrast, these small precipitates are cobalt-enriched particles. The TEM observation (see the rectangle in the upper right corner of the Fig. 2c) also confirmed the presence of these precipitates. However, the measurements of chemical composition showed no differences between the matrix and separate precipitates. This is probably related to the small size of the precipitates (less than 100 nm) in relation to the thickness of the foil.

The phase diagram suggests that increasing the annealing temperature up to 685 °C (Fig. 1) leads to higher cobalt content in the α-solid solution, and a slight decrease of the amount of Ti_2Co intermetallic phase. This is in a good correlation with experimental data, obtained by XRD analysis (Fig. 3). Based on the XRD diffraction patterns, it was found that the α-phase peaks in the sample annealed at 600 °C were shifted towards the higher diffraction angles in comparison to the samples annealed at lower temperatures. This is indicative of a decrease in lattice parameter values (Table 1) because of Co content increase in the α-phase [19]. It can be seen that lower lattice parameters of the α-phase were observed in the sample annealed at 600 °C, and the higher ones correspond to the sample annealed at 400 °C. Moreover, the lower the temperature of annealing, the higher the c/a ratio, which is beneficial for the α → ω transformation due to primary "basal" dislocation slip during shear deformation. Thus, the amount of Co dissolved in the α-phase matrix rises with increasing annealing temperature. Since the total amount of cobalt remains the same (3.3 at.% Co), the cobalt atoms migrate for the formation of α-phase from Ti_2Co particles, and their the volume fraction decreases slightly as annealing temperature rises. It should be noted that the maximum Co solubility in the α-phase (0.86 at. % Co) could be reached at a eutectoid reaction temperature close to 685 °C [20].

Table 1
Lattice parameters of the α- and ω-phases before and after HPT, as well as the volume fraction of the ω-phase after HPT process.

Sample	Lattice parameter, Å			Volume ffraction of the ω-phase, %
	Before HPT	After HPT		
	α-Ti	α-Ti	ω-Ti	
Ti–3.3 at.% Co 400 °C, 5685 h	$a = 2.954 \pm 0.001$ $c = 4.759 \pm 0.001$ $c/a = 1.611$	$a = 2.966 \pm 0.001$ $c = 4.718 \pm 0.0001$ $c/a = 1.591$	$a = 4.622 \pm 0.001$ $c = 2.833 \pm 0.001$	80
Ti–3.3 at.% Co 500 °C, 5685 h	$a = 2.953 \pm 0.001$ $c = 4.729 \pm 0.001$ $c/a = 1.602$	$a = 2.963 \pm 0.0001$ $c = 4.725 \pm 0.0001$ $c/a = 1.595$	$a = 4.622 \pm 0.001$ $c = 2.833 \pm 0.001$	65
Ti–3.3 at.% CoC 600 °C, 2774 h	$a = 2.941 \pm 0.001$ $c = 4.689 \pm 0.001$ $c/a = 1.591$	$a = 2.957 \pm 0.001$ $c = 4.703 \pm 0.001$ $c/a = 1.590$	$a = 4.622 \pm 0.001$ $c = 2.833 \pm 0.001$	5
Pure Ti	$a = 2.955 \pm 0.001$ $c = 4.694 \pm 0.001$ $c/a = 1.588$ [19]	$a = 2.959 \pm 0.001$ $c = 4.690 \pm 0.001$ $c/a = 1.585$ [19]	$a = 4.627 \pm 0.001$ $c = 2.830 \pm 0.001$	40 [10]

SEM micrographs of the samples after HPT are shown in Fig. 4. It can be seen that the morphology of HPT-deformed Ti_2Co particles differs with pre-annealing temperature. The particles after deformation of the samples, pre-annealed at 500 and 600 °C, are characterized by a larger grain size, a more regular shape and clearly developed boundaries (Fig. 4 e, f). In the pre-annealed at 400 °C sample, (Fig. 4d) these particles were distinctly elongated along the small transverse dimension and their boundaries were blurred. Thereby, it seems, that in the case of higher pre-annealing temperatures, Ti_2Co particles were less refined and less dissolved under HPT treatment than the smaller ones observed in the sample pre-annealed at 400 °C.

XRD patterns obtained after HPT (Fig. 5) showed that all the α-phase peaks were broader and their intensity was significantly lower. This is associated with the strong grain refinement of the deformed matrix and significant micro-distortion of the crystal lattice, typical for materials subjected to SPD. Peak broadening was also observed in the Ti_2Co intermetallic phase. However, the intensity was strongly related to pre-annealing temperature. At 600 °C, the reflections belonging to Ti_2Co appear distinctly, but at 400 °C they are almost absent. This suggests that the maximal dissolution of Ti_2Co particles is observed at lower temperatures. Moreover, the ω-phase (designated as triangle in the XRD patterns) appeared in all deformed samples. The crystallographic mechanism of the α → ω phase transformation implies shear deformation along the (00.1)α planes [20]. The XRD patterns show that the strong (00.2) peak of the α-phase completely disappeared, and the high

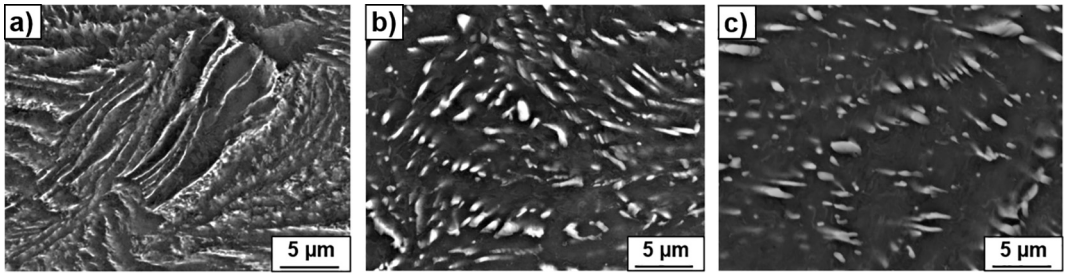

Fig. 4. SEM images of the microstructure of the HPT-deformed Ti–3.3 at.% Co alloy, pre-annealed at 400 (a), 500 (b) and 600 °C (c).

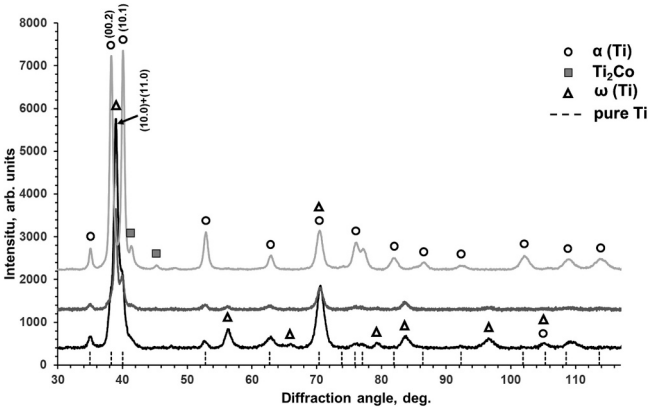

Fig. 5. X-ray diffraction patterns of the Ti–3.3 at.% Co alloy after annealing and HPT.

intensity (10.0 + 11.0) doublet of the ω-phase appeared after HPT in the sample pre-annealed at 400 °C. This confirms the α-to-ω transformation mechanism observed earlier in pure Ti under HPT conditions [22]. On the other hand, the intensity of the (10.1) α-phase peak is significantly lower. A similar situation is observed in the sample pre-annealed at 500 °C, while only two α-phase peaks, (00.2) and (10.1), are observed without the appearance of ω-phase peaks in the diffraction angles between 37 and 41° in the sample pre-annealed at 600 °C (Fig. 5). This means that the α → ω phase transformation was suppressed in this sample. The volume fraction of the ω-phase was calculated on the basis of the XRD patterns. It was about 80%, 65% and ≤ 5% in the samples pre-annealed at 400, 500 and 600 °C, respectively (Table 1). So, the lower the temperature of pre-annealing, the greater the volume fraction of the ω-phase after HPT. It should be noted that HPT-induced volume fraction of the ω-phase reached only ~40% in pure Ti deformed at the same conditions of HPT [10]. as This means that alloying of Ti with *d*-electron rich transition elements such as Co, Nb [23] or Fe [10] increases the ω-phase fraction induced by HPT in comparison with pure Ti. The decreased ω-phase amount at higher pre-annealing temperatures can be indirectly driven by the change of the amount and morphology of intermetallic particles, the morphology of the α-grains, and the cobalt content in the α-grains of the Ti-3.3 at.% Co alloy.

The HPT deformation of pure Ti results in a decrease of the parameter *c* and an increase of the parameter *a* (Table 1). The similar situation is observed after HPT of the examined Ti–3.3 at.% Co alloy, except for the sample preliminarily annealed at 600 °C, where an increase in both parameters *a* and *c* was observed (Table 1). Even though, this sample (600 °C) exhibits the minimum values of *a* and *c* parameters after HPT. It means that the deformed α-phase retains an increased content of cobalt as compared with other samples. On the other hand, finer Ti_2Co precipitates formed at lower temperatures (400 and 500 °C) should be easily dissolved into the matrix by HTP. The question therefore arises, where is the location of cobalt derived from the partial dissolution of intermetallic Ti_2Co particles? Most probable, the dissolved by HPT cobalt migrates directly into the ω-phase, since the solubility of the second element is higher in the ω-phase than in the matrix [22,24]. This is well in line with experimental observations as the sample preliminarily annealed at 600 °C, contains the smallest amount of the ω-phase (only 5% due to the α-phase supersaturated with cobalt) as well as shows the minimum dissolution of intermetallic particles.

The bright field and dark field TEM images, as well as the SAED patterns of the deformed samples, are presented in Fig. 6. Analysis of SAED patterns (c, f, i) indicated larger volume fraction of the ω-phase and stronger grain refinement of the α- and ω-phases, especially at lower pre-annealing temperatures. The contrast in the BF image is related to the diffraction contrast – the grains oriented along the electron beam are dark. The bright grains visible on the DF correspond to the reflections selected on the ring diffraction pattern by objective aperture. Unfortunately, the morphology of the small α- and ω-phase grains is identical, which makes them difficult to distinguish. The white rings inserted in the diffraction patterns show the positions of the objective aperture for obtaining dark-field images. In other words, these white rings indicate a set of reflexes coming from α- and ω-phases, corresponding to bright grains in a dark field image (Fig. 6b, e, h). During the preparation of the foils by electropolishing, intermetallic Ti_2Co particles fell out of the material, therefore the images in Fig. 6 a-i represent only a deformed matrix without intermetallic particles. The microstructure of the sample pre-annealed at 600 °C was non-uniform: a mixture of fine-grained α- and ω-phases and large α-phase grains were observed. Moreover, a particle of Ti_2Co phase was also noticed (Fig. 6 j-l). The grain size of the fine (α + ω) mixture reached about 70 nm, 100 nm and 150 nm for 400, 500 and 600 °C, respectively.

The thermal stability of the metastable ω-phase was studied by means of the DSC technique and *in situ* high-temperature XRD measurements. In the case of the DSC technique, deformed samples were heated to 800 °C at the rate of 20 °C/min. The DSC heating curves of the deformed Ti–3.3 at.% Co alloy are presented in Fig. 7. According to the Ti—Co phase diagram, the endothermic peaks observed in the temperature range of 680–720 °C are attributed to the dissolution of the Ti_2Co phase. Exothermic peaks in the temperature range of 360–460 °C, especially clearly visible for the samples pre-annealed at 400 and 500 °C (Fig. 7b), can be associated with the reverse ω → α phase transformation. The ω-phase is the metastable one, and this reverse ω → α transformation is observed as an exothermic process. It can be seen that the areas under the exothermic peaks correspond to the amount of the ω-phase. The maximal exothermic peak was observed in the sample pre-annealed at 400 °C, where the ω-phase amount was maximal. This exothermic peak was not observed in the sample pre-annealed at 600 °C, where the ω-phase amount was only about 5%. The endothermic peak observed at the temperature range of 480–560 °C in this sample can be associated with homogenisation of chemical composition of the deformed material.

In situ XRD maps (measured with the step of heating 5 °C/min) of the deformed samples are presented in Fig. 8. As the acquisition time for each pattern was 80 min. preceded by 10 min. for temperature stabilisation, the measurements can be considered as conducted in quasi-equilibrium conditions. Before heating, the (11.0) peak of the ω-phase and the (10.1) peak of the α-phase can be distinguished in the 34–42°

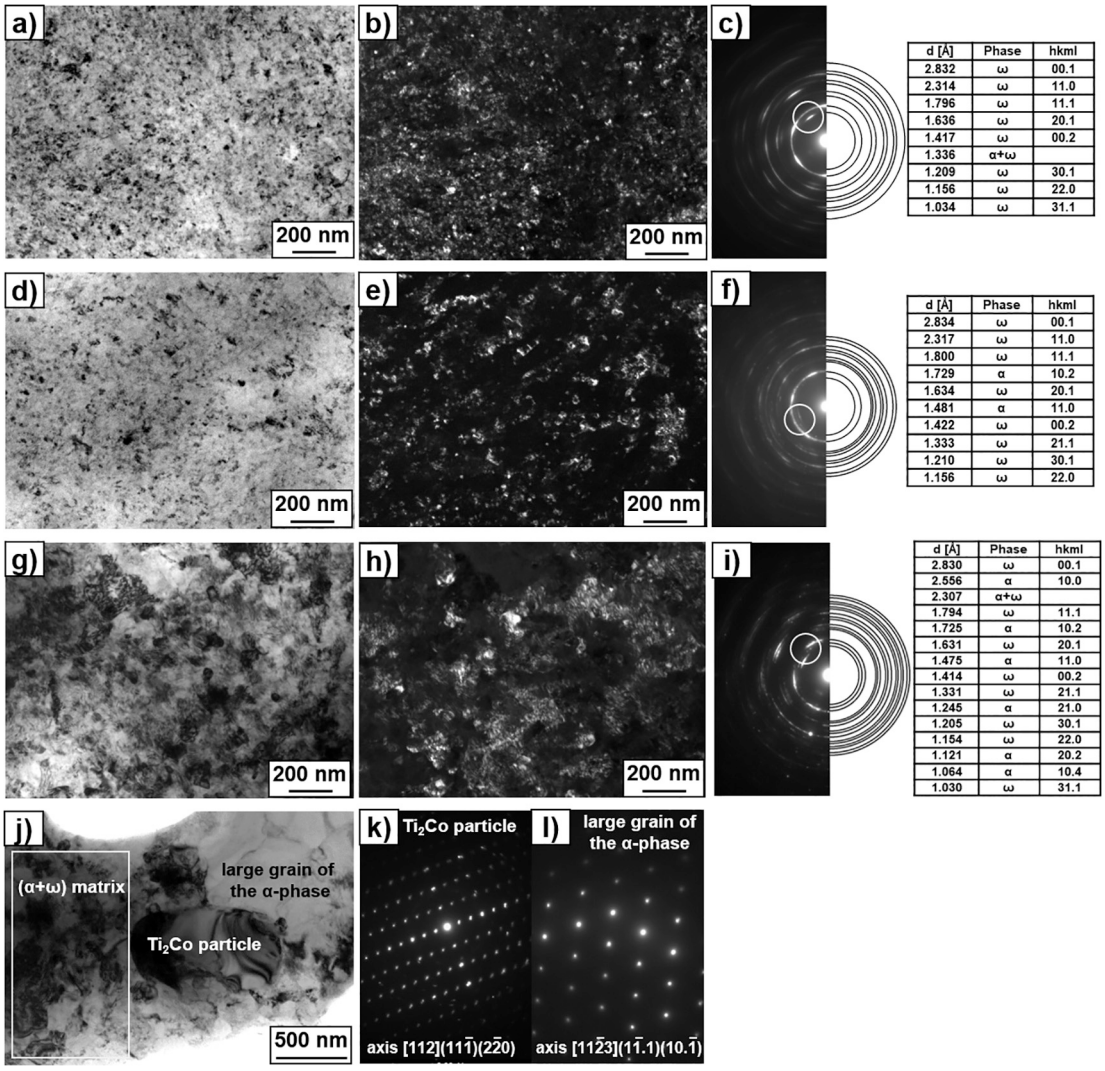

Fig. 6. TEM images of the microstructure of the HPT-deformed Ti–3.3 at.% Co alloy, pre-annealed at 400 (a-c), 500 (d-f) and 600 °C (g-m). Bright field (a, d, g, j) and dark field (b, e, h, k) images, as well as the SAED patterns (the positions of the objective aperture for obtaining dark-field images are marked) with the solutions in Tables (c, f, i) and the SAED patterns (k, i) of the Ti2Co particle and α grain, marked in (j).

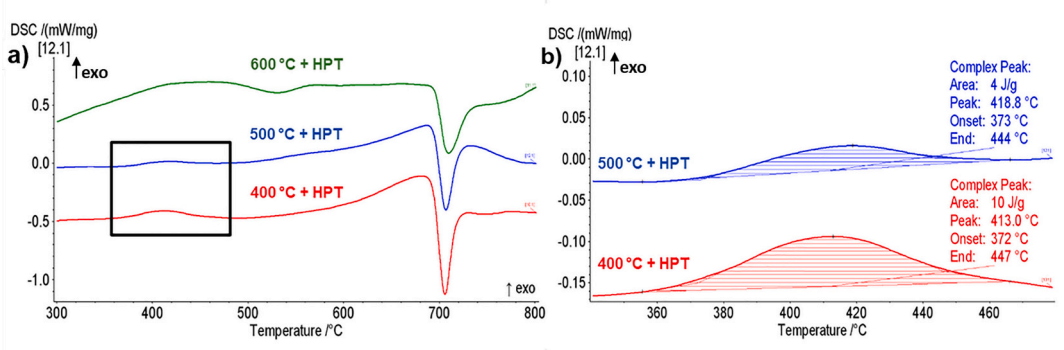

Fig. 7. The DSC heating curves of the Ti–3.3 at.% Co alloy after annealing and HPT deformation (a). Enlarged part of the DSC heating curves (b) marked as black rectangle in (a).

range of 2θ angles. The weakly pronounced (10.0) peak of the α-phase before heating (visible on the standard XRD curves in Fig. 5) is related to different XRD times. For the *in situ* method, there is not enough time to register many X-ray counts compared to the standard method. The analysis of the XRD *in situ* maps showed that the heating of the deformed samples (especially pre-annealed at 400 and 500 °C) up to 325 °C resulted in the complete disappearance of the ω-phase, amplification of the (10.0) and (10.1) α-phase peaks as well as the appearance of the peak from the Ti_2Co phase. Therefore, the decomposition of the ω-phase into the α- and Ti_2Co-phases is observed. The appearance of the Ti_2Co phase

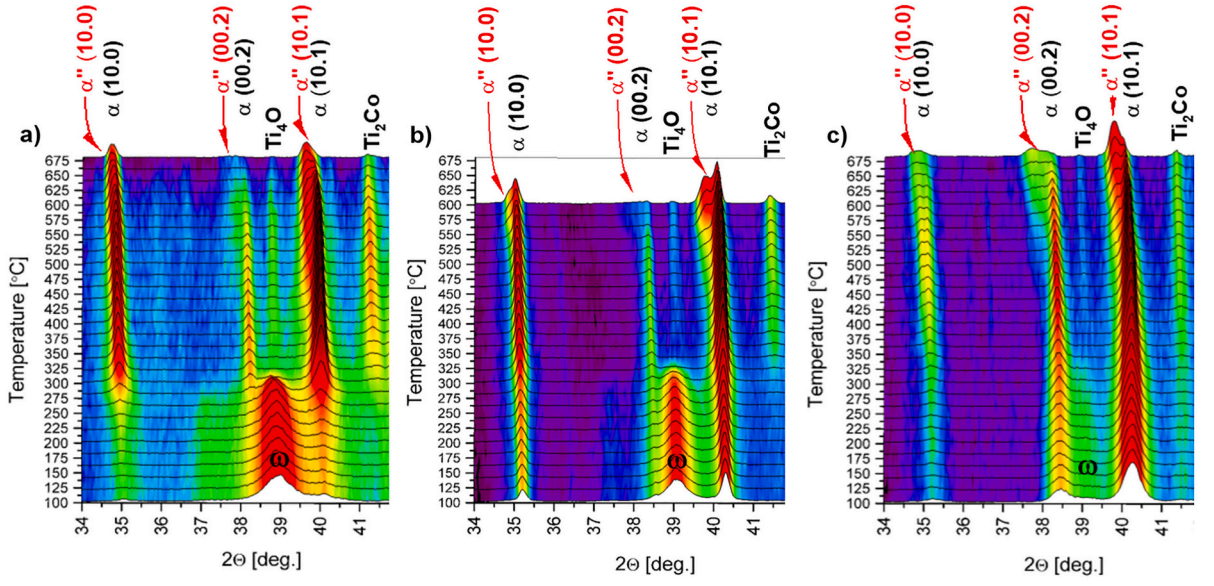

Fig. 8. The XRD *in situ* heating maps of the deformed Ti–3.3 at.% Co alloy, pre-annealed at 400 (a), 500 (b) and 600 °C (c). At the given interval, the ω-phase is presented by (10.0 + 11.0) doublet of peaks.

also explains the gradual growth of the DSC heating curves in the range between decomposition of the ω-phase and dissolution of the Ti_2Co phase (Fig. 7). Since the ω-phase is enriched in cobalt as an alloying element (by analogy with the ω-phase enriched in iron in Ti—Fe alloys [22,24]), it is assumed that the α-phase arising after the decomposition of the ω-phase, is also enriched in cobalt.

Analysis of the XRD *in situ* maps showed also that heating to the highest temperatures resulted in a slight shift of α-phase peaks towards the lower diffraction angles, and the split of these peaks. The most noticeable effect occurred in regard to the (10.1) α-phase peak of higher intensity (Fig. 8). The shift of the α-phase peaks to lower diffraction angles indicates the increase of the lattice parameters due to thermal expansion. On the other hand, the split of the (10.1) α-phase peak (or appearance of the new (10.1) α-phase peak (singed as α′ in the Fig. 8) near the main (10.1) α-phase peak can be associated with the appearance of the new α-phase with lower cobalt content.

Dependence of the α-phase lattice parameters on the heating temperature during *in situ* XRD measurement is presented in Fig. 9. The lower temperature of pre-annealing of the deformed samples led to the higher parameter *a* of the α-phase. This correlates well with the data obtained from the standard XRD method (see Table 1). Four stages can be observed during the heating of the HPT-deformed sample pre-annealed at 400 °C. At the first stage, the decrease of parameter *a* is observed from 2.963 to 2.958 Å in the temperature range 100–140 °C. Generally, HPT (even HPT of pure Ti) resulted in the increase of the parameter *a* and decrease of the parameter *c* (see Table 1). It is possible that, during the first heating stage, a relaxation of the internal stresses occurs, resulting in the decrease of the parameter *a* and increase of the parameter *c*. In the second stage of heating, up to 260 °C, the increase the parameter *a* up to 2.966 Å is observed. This is probably related with the thermal expansion of the crystal lattice. The next sharp decrease of the *a* from 2.966 to 2.961 Å during heating to 300 °C is attributed to the appearance of the α-phase enriched in Co due to the ω → α phase transformation. The next heating to 600 °C again leads to an increase of the parameter *a* as the result of thermal expansion of the crystal lattice. At a temperature of 540 °C, there was a new α′′-phase, free of cobalt, with the highest parameters of *a* and *c*, marked red in Fig. 9. It should be noted that the presence of the new α′′-phase is observed in every sample at the same temperatures, and that parameters *a* and *c* of this phase are larger than for pure Ti (Table 1) due to thermal lattice expansion. In the deformed sample pre-annealed at 500 °C, only three stages on the curve of the parameter *a* can be distinguished. The first one (in the temperature range of 20–100 °C) is also connected with the relaxation of the internal stresses. The second one (between 100 and 340 °C) and the third one (between 340 and 600 °C) are connected with the thermal expansion of the crystal lattice. The absence of a drop in parameter *a* between the second and the third stages is probably related with the least ω-phase content in comparison to the sample pre-annealed at 400 °C. In the sample pre-annealed at 600 °C, where the amount of the HPT-induced ω-phase is ~5%, only a monotonic increase of the parameter *a* is observed in the entire range of the heating. The increase of parameter *c* of the α-phase is observed in the all samples during heating from 20 to 600 °C, due to thermal expansion of the crystal lattice.

The thermal stability of the ω-phase and the microstructure transformations were studied by DSC and *in situ* XRD methods. Additional details worthy of further discussion were discovered. For *in situ* XRD measurement, the temperature range of ω-phase decomposition is significantly shifted towards the lower temperatures in comparison to the data obtained from the DSC examination. This is related to the various heating rates applied in both experiments. For example, DSC heating at different rates (20, 10 and 5 °C/min) showed that, the lower the heating rate, the stronger the shift of the ω-phase decomposition range towards lower temperatures (Fig. 10). The shift of the temperature range of the ω → α reverse phase transformation, depending on the heating rate, may indicate the diffusion nature of this transformation, or the contribution of a diffusion process to the transformation [21]. It should be noted that the mechanism of this transformation has not yet been fully studied and documented in the literature. T. Low and S. Niezgoda [25] claimed that the ω → α transformation is hindered by defects in the ω-phase. They found a significant reduction of dislocation densities in the ω- phase prior to initiation of the reverse ω → α transformation. Since the annihilation of dislocation is a thermally-activated process, it could make a noticeable contribution to observed phase transformation.

It should be noted that the α → ω and β → ω phase transformations are martensite-type (diffusionless). For example, the HPT of pure BT1–0 titanium at room and cryogenic temperatures resulted in α → ω martensite-type phase transformation [26]. Less deformation has to be applied to transform the same amount of ω-phase at room temperature than at 77 K. Therefore, it seems that thermally activated processes also play a role in the nucleation of the ω-phase [26].

It should be noted that HPT-induced ω-phase volume fraction in pure

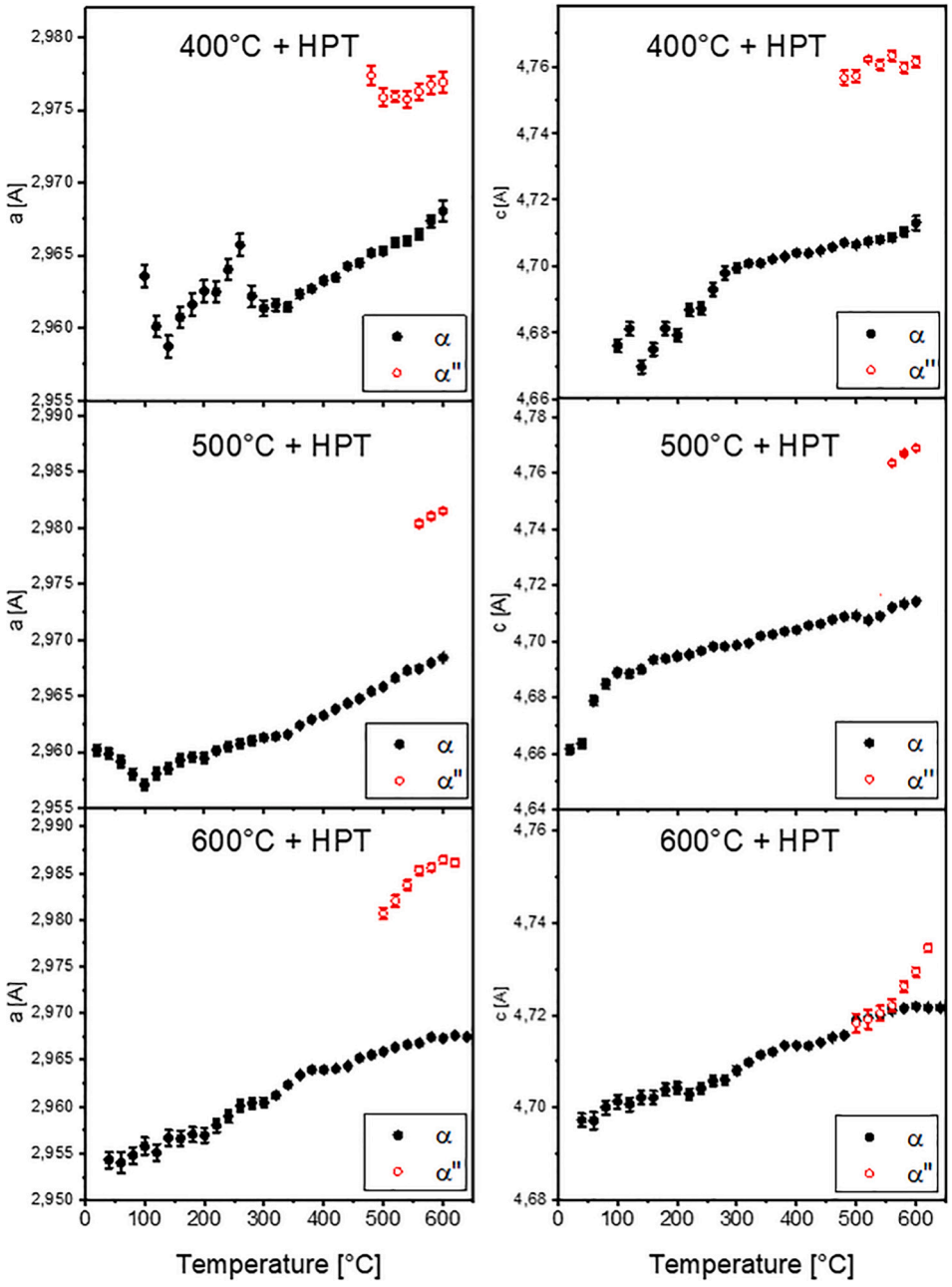

Fig. 9. The graphs of dependence of crystal lattice parameters (*a* and *c*) of the α-phase on the temperature of heating.

Ti (under the same conditions) reached only approximately 40% [10], and the process of reverse ω → α transformation, is finished at 180 °C for the heating at a rate of 10 °C /min [23]. Therefore, the alloying with 3.3 at.% of Co results in the significant increase of volume fraction of the ω-Ti phase and its thermal stability. The same situation was observed in the Ti-based alloys with 1, 2, 4 and 7 wt% Fe [27], where the amount of the ω-phase induced by HPT reached about 50%, 80%, 94% and 72%, respectively. The thermal stability of the ω-phase was studied using DSC measurements with the heating rate of 10 °C/min and *in situ* XRD. It was found that (1) the process of the decomposition of the ω-phase is exothermic, (2) the ω-phase completely decomposes slightly above 500 °C in all studied iron concentrations [27]. In other words, the iron-doped ω-phase decomposes even at higher temperature than the cobalt-doped one.

The microhardness of the samples annealed at 400, 500 and 600 °C was found to be 2.4 ± 0.2, 2.0 ± 0.1 and 3.9 ± 0.3 GPa, respectively. As the size of the indenter imprint was about 20 μm, the measured hardness was true for the Ti_2Co particles together with the surrounding matrix. The sample annealed at 400 °C has a slightly higher hardness in comparison to the sample annealed at 500 °C. This can be explained by the specific morphology of Ti_2Co particles, which formed a cellular structure network (Fig. 2d). A significant increase of the hardness (almost two-fold) in the sample annealed at 600 °C is likely to be related to the effect of dispersion hardening from the nano precipitates observed in the α-phase matrix (Fig. 2c). The hardness values after HPT, measured along the radius from the centre to the edge of the deformed discs, are presented in Fig. 11. The monotonic increase of hardness is observed along the radius from the centre to the edge of the deformed samples. This is typical for the HPT samples. In addition, the hardness curves of all deformed samples almost coincide with each other, especially the curves of the samples pre-annealed at 400 and 600 °C. However, the maximum hardness increase is observed only in the samples pre-annealed at 400 and 500 °C, due to the larger volume fraction of the hard ω-phase and grain refinement of microstructure. For example, the hardness of these

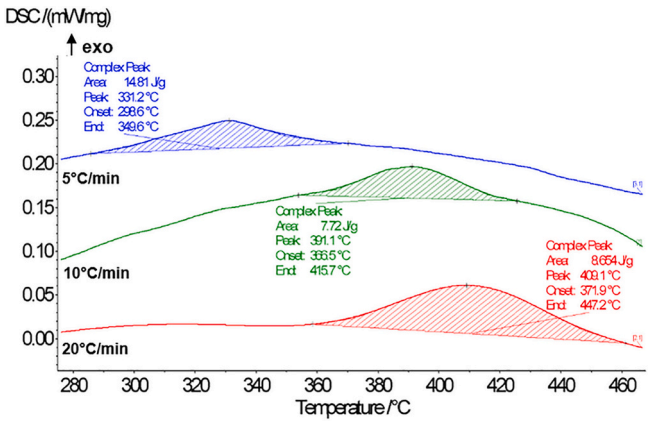

Fig. 10. The DSC heating curves of the deformed Ti–3.3 at.% Co alloy (pre-annealed at 400 °C) at different rates of heating.

samples, measured at a distance 2.6 mm from the centre of the deformed disc, increased from 2.4 to 6.0 GPa and from 2.0 to 5.8 GPa, respectively (Fig. 11). The minimum increase in hardness (from 3.9 to 6.0 GPa) is observed in the sample pre-annealed at 600 °C due to only grain refinement of microstructure.

4. Conclusions

The Ti–3.3 at.%Co alloy was annealed below the temperature of eutectoid transformation in order to obtain a mixture of α- and Ti_2Co intermetallic phases. Subsequent HPT deformation resulted in: (1) strong grain refinement of the microstructure, (2) fragmentation and partial dissolution of Ti_2Co intermetallic phase, and (3) α → ω phase transformation. The lower temperature of pre-annealing led to stronger grain refinement, greater effect of Ti_2Co phase dissolution, and formation of higher volume fraction of the high-pressure ω-phase. It is possible that HPT-induced α → ω phase transformation depends on the cobalt content in the initial α-phase, and morphology of microstructure. In other words, lower cobalt content and smaller grain size of the α- and Ti_2Co-phases leads to a higher amount of ω-phase induced by HPT.

In situ high-temperature XRD revealed the temperature ranges of ω-phase stability and the following transformation of microstructure. Alloying titanium with 3.3 at.% of cobalt results in a significant increase of the volume fraction of the ω-phase and its thermal stability, from 180°C to 415°C, in comparison to pure titanium. It is possible that the recovery and annihilation of high-density defects in the ω-phase contributes to phase transformation.

The samples pre-annealed at 400 and 500 °C showed the maximum increase in hardness after HPT due to the large amount of the ω-phase, and to microstructure grain refinement.

Data availability statement

The raw/processed data required to reproduce these findings cannot be shared at this time as the data also forms part of an ongoing study.

Declaration of Competing Interest

The authors declare that they have no known competing financial interests or personal relationships that could have appeared to influence the work reported in this paper.

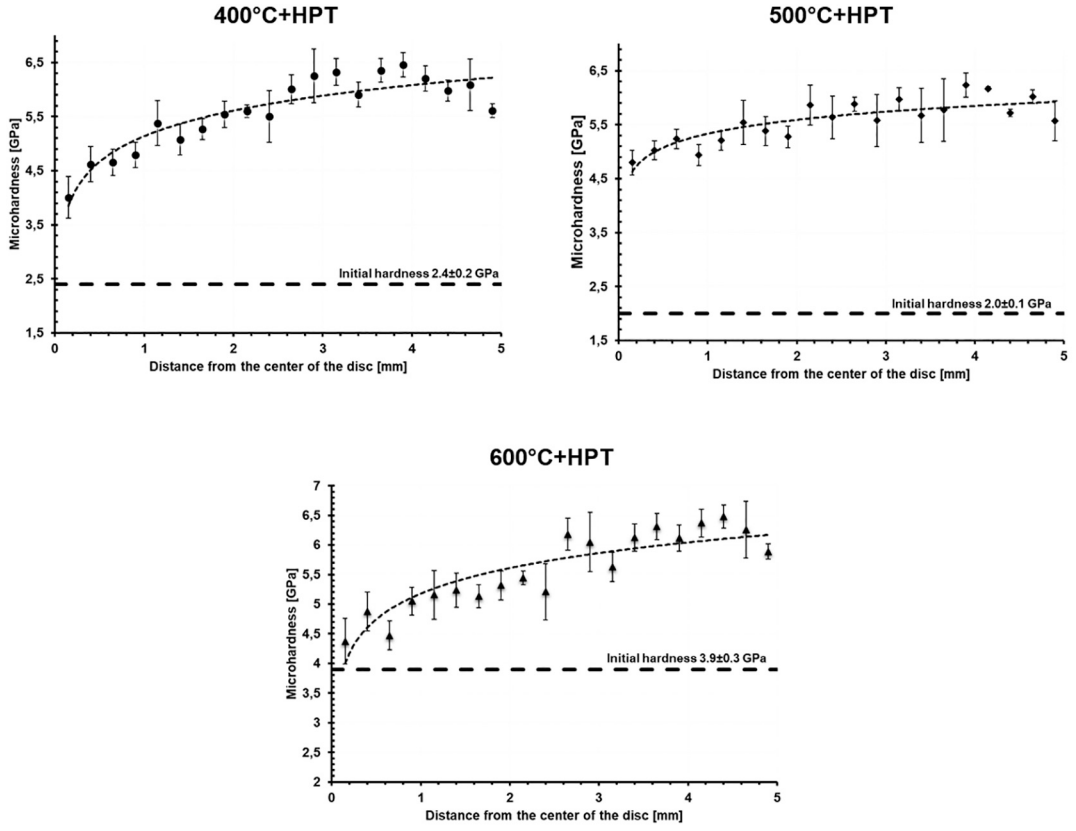

Fig. 11. The graphs of microhardness measured along the radius of the deformed Ti-3.3 at.% Co alloy. The logarithmic trend line is presented in the graphs (as a guide for your eyes).

Acknowledgements

This work is supported by National Science Centre of Poland (grant OPUS 2017/27/B/ST8/0 1092) and Russian Foundation for Basic Research (grants 18-03-00067, 19-58-06002) as well as state task of ISSP RAS. SEM and TEM investigations were performed within the Accredited Testing Laboratories possessing the certificate No. AB 120 issued by the Polish Centre of Accreditation according to European standard PN-ISO/IEC 17025:2005 and the EA-2/15.

References

[1] K. Wang, The use of titanium for medical applications in the USA, Mater. Sci. Eng. A 213 (1996) 134–137, https://doi.org/10.1016/0921-5093(96)10243-4.
[2] J. Onagawa, Preparation of high corrosion resistant titanium alloys by spark plasma sintering, J. Jpn. Inst. Metals 63 (1999) 1149–1152, https://doi.org/10.2320/jinstmet1952.63.9_1149.
[3] Q. Liu, W.Y. Yang, G.L. Chen, On superplasticity of two phase alpha-titanium-intermetallic Ti–(Co, Ni)–Al alloy, Acta Metall. Mater. 43 (1995) 3571–3582, https://doi.org/10.1016/0956-7151(95)00032-Q.
[4] V. Stolyarov, R. Lapovok, I. Brodova, P. Thomson, Ultrafine-grained Al–5 wt.% Fe alloy processed by ECAP with backpressure, Mater. Sci. Eng. A 357 (2003) 159–167, https://doi.org/10.1016/S0921-5093(03)00215-6.
[5] B. Straumal, A. Korneva, P. Zięba, Phase transitions in metallic alloys driven by the high pressure torsion, Arch. Civ. Mech. Eng. 14 (2014) 242–249, https://doi.org/10.1016/j.acme.2013.07.002.
[6] S. Ohsaki, S. Kato, N. Tsuji, T. Ohkubo, K. Hono, Bulk mechanical alloying of Cu–Ag and Cu/Zr two-phase microstructures by accumulative roll-bonding process, Acta Mater. 55 (2007) 2885–2895, https://doi.org/10.1016/j.actamat.2006.12.027.
[7] A.V. Sergueeva, C. Song, R.Z. Valiev, A.K. Mukherjee, Structure and properties of amorphous and nanocrystalline NiTi prepared by severe plastic deformation and annealing, Mater. Sci. Eng. A 339 (2003) 159–165, https://doi.org/10.1016/S0921-5093(02)00122-3.
[8] A.M. Glezer, M.R. Plotnikova, A.V. Shalimova, S.V. Dobatkin, Severe plastic deformation of amorphous alloys: I. Structure and mechanical properties, Bull. Russ. Ac. Sci. Phys 73 (2009) 1233–1239.
[9] X.L. Wang, L. Li, W. Mei, W.L. Wang, J. Sun, Dependence of stress-induced omega transition and mechanical twinning on phase stability in metastable β Ti–V alloys, Mater. Charact. 107 (2015) 149–155, https://doi.org/10.1016/j.matchar.2015.06.038.
[10] A.R. Kilmametov, Yu. Ivanisenko, A.A. Mazilkin, B.B. Straumal, et al., The α→ω and β→ω phase transformations in Ti-Fe alloys under high-pressure torsion, Acta Mater. 144 (2018) 337–351, https://doi.org/10.1016/j.actamat.2017.10.051.
[11] A.K. Singh, M. Mohan, C. Divakar, Pressure-induced alpha-omega transformation in titanium: features of the kinetics data, J. Appl. Phys. 54 (1983) 5721–5730, https://doi.org/10.1063/1.331793.
[12] S.C. Gupta, K.D. Joshi, S. Banerjee, Experimental and theoretical investigations on d and f electron systems under high pressure, Metall. Mater. Trans. A 39 (2008) 1593–1601, https://doi.org/10.1007/s11661-007-9377-1.
[13] J.R. Patel, M. Cohen, Criterion for the action of applied stress in the martensitic transformation, Acta Mettal. 1 (1953) 531–538, https://doi.org/10.1016/0001-6160(53)90083-2.
[14] N. Adachi, Y. Todaka, K. Irie, M. Umemoto, Phase transformation kinetics of x-phase in pure Ti formed by high-pressure torsion, J. Mater. Sci. 51 (2016) 2608–2615, https://doi.org/10.1007/s10853-015-9574-z.
[15] M.J. Kriegel, A. Kilmametov, M. Rudolph, B.B. Straumal, A.S. Gornakova, et al., Transformation pathway upon heating of Ti–Fe alloys deformed by high-pressure torsion, Adv. Eng. Mater. 20 (2018) 1700933, https://doi.org/10.1002/adem.201700933.
[17] A. Korneva, B. Straumal, A. Kilmametov, Ł. Gondek, A. Wierzbicka-Miernik, et al., Thermal stability and microhardness of metastable ω-phase in the Ti-3.3 at.% Co alloy subjected to high pressure torsion, J. Alloys Compd. 834 (2020) 155132, https://doi.org/10.1016/j.jallcom.2020.155132.
[18] J. Rodriguez-Carvajal, Recent advances in magnetic structure determination by neutron powder diffraction, Physica B 192 (1993) 55–69, https://doi.org/10.1016/0921-4526(93)90108-I.
[19] B.B. Straumal, A.R. Kilmametov, Yu. Ivanisenko, A.A. Mazilkin, R.Z. Valiev, N. S. Afonikova, A.S. Gornakova, H. Hahn, Diffusive and displacive phase transitions in Ti–Fe and Ti–Co alloys under high pressure torsion, J. Alloys Compd. 735 (2018) 2281–2286, https://doi.org/10.1016/j.jallcom.2017.11.317.
[20] J.L. Murray, The Co-Ti (cobalt-titanium) system, Bull. Alloy Phase Diagr. 3 (1982) 74–85.
[21] D.R. Trinkle, R.G. Hennig, S.G. Srinivasan, et al., New mechanism for the α to ω martensitic transformation in pure titanium, Phys. Rev. Lett 91 (2003) 025701, https://doi.org/10.1103/PhysRevLett.91.025701.
[22] Y. Ivanisenko, A. Kilmametov, H. Rösner, R.Z. Valiev, Evidence of α→ω phase transition in titanium after high pressure torsion, Int. J. Mater. Res. 99 (2008) 36–41, https://doi.org/10.3139/146.101606.
[23] A. Panigrahi, M. Bönisch, T. Waitz, E. Schafler, M. Calin, J. Eckert, W. Skrotzki, M. Zehetbauer, Phase transformations and mechanical properties of biocompatible Ti–16.1Nb processed by severe plastic deformation, J. Alloys Compd. 628 (2015) 434–441, https://doi.org/10.1016/j.jallcom.2014.12.159.
[24] A. Kilmametov, Yu. Ivanisenko, B. Straumal, A.A. Mazilkin, et al., Transformations of α' martensite in Ti–Fe alloys under high pressure torsion, Scr. Mater. 136 (2017) 46–49, https://doi.org/10.1016/j.scriptamat.2017.04.010.
[25] T.S.E. Low, S.R. Niezgoda, Modeling the α/ω thermal stability in shocked Zr: a coupling between dislocation removal and phase transformation, Acta Mater. 156 (2018) 104–115, https://doi.org/10.1016/j.actamat.2018.06.004.
[26] N.A. Shurygina, A.O. Cheretaeva, A.M. Glezer, D.L. D'yakonov, I.V. Chshetinin, et al., Effect of the temperature of megaplastic deformation in a Bridgman chamber on the formation of structures and the physicochemical properties of titanium (BT1–0), Bull. Russ. Acad. Sci. Phys. 82 (2018) 1113–1124, https://doi.org/10.3103/S1062873818090204.
[27] M.J. Kriegel, A. Kilmametov, M. Rudolph, B.B. Straumal, A.S. Gornakova, et al., Transformation pathway upon heating of Ti–Fe alloys deformed by high-pressure torsion, Adv. Eng. Mater. 20 (2018) 1700933, https://doi.org/10.1002/adem.201700933.
[28] M Wojdyr, Fityk: A general-purpose peak fitting program, J. Appl. Crystallogr. 43 (2010) 1126–1128, https://doi.org/10.1107/S0021889810030499.